Eur. Phys. J. B **31**, 125–139 (2003)
DOI: 10.1140/epjb/e2003-00016-8

THE EUROPEAN PHYSICAL JOURNAL B

Proximity effect in multiterminal hybrid structures

H. Jirari, R. Mélin[a], and N. Stefanakis

Centre de Recherches sur les Très basses températures (CRTBT)[b], BP 166X, 38042 Grenoble Cedex, France

Received 6 May 2002 / Received in final form 20 November 2002
Published online 27 January 2003 –

Abstract. We consider the proximity effect in multiterminal ferromagnet/superconductor (FSF) hybrid structures in which two or three electrodes are connected to a superconductor. We show that two competing effects take place in these systems: (i) pair breaking effects due to the response to the exchange field induced in the superconductor; (ii) a reduction of the superconducting order parameter at the interface that takes place already in NS junctions. We focus on this second effect that dominates if the thickness of the S layer is small enough. We consider several single-channel electrodes connected to the same site. We calculate the superconducting order parameter and the local density of state (LDOS). With two ferromagnetic electrodes connected to a superconductor we find that the superconducting order parameter in the ferromagnetic alignment is larger than the superconducting order parameter in the antiferromagnetic alignment ($\Delta_{\rm F} > \Delta_{\rm AF}$), in agreement with [Eur. Phys. J. B **25**, 373 (2002)]. If a third spin polarized electrode is connected to a superconductor we find that $\Delta_{\rm F} - \Delta_{\rm AF}$ can change sign as the transparency of the third electrode increases. This can be understood from the fact that the superconducting order parameter is reduced if pair correlations among the ferromagnetic electrodes increase. If the two ferromagnetic electrodes are within a finite distance we find Friedel oscillations in the Gorkov function but we still obtain $\Delta_{\rm F} > \Delta_{\rm AF}$.

PACS. 74.80.Fp Point contacts; SN and SNS junctions – 72.10.Bg General formulation of transport theory – 74.50.+r Proximity effects, weak links, tunneling phenomena, and Josephson effects – 74.80.Dm Superconducting layer structures: superlattices, heterojunctions, and multilayers

1 Introduction

The manipulation of entangled states of electrons in condensed matter devices has focussed an important interest recently. The ground state of a superconductor is a condensate of Cooper pairs that form singlet states. Entangled states of electrons can thus be manipulated in transport experiments by extracting Cooper pairs out of a superconductor. Several experiments using a superconductor as a source of entangled states of electrons have been proposed recently. For instance it was shown in reference [1] that entangled states of electrons can be manipulated in a double dot experiment. A quantum teleportation experiment using three quantum dots has been proposed recently [2]. Another possible experiment has also been proposed in reference [3] in which a "beam splitter" is connected to a superconductor. In this situation noise correlations can reveal information about electronic entanglement [3]. Other possible experiments in which several ferromagnetic electrodes are connected to a superconductor have been investigated theoretically in references [4–8].

There is a rich physics occurring at a single ferromagnet/superconductor (FS) interface. For instance Andreev reflection is suppressed if the spin polarization of the ferromagnetic metal increases. This is because the incoming electron and the reflected hole belong to different spin bands. As a consequence Andreev reflection can occur only in the channels having both a spin-up and a spin-down Fermi surface [9]. This theoretical prediction was well verified in experiments [10,11] and it was shown that with high transparency interfaces the suppression of Andreev reflection by spin polarization can be used to probe the Fermi surface polarization [10]. The results of the Andreev reflection experiments compare well with another method based on spin polarized tunneling in the presence of Zeeman splitting [12]. Another phenomenon taking place at FS interfaces is that the pair amplitude induced in a ferromagnetic metal can oscillate in space. This gives the possibility of fabricating π junctions in which the Josephson relation changes sign [13–19]. It is also well established that FS multilayers present oscillations of the superconducting critical temperature as the thickness of the ferromagnetic layer is varied [20–25]. Other new phenomena related to the proximity effect have also been investigated in diffusive FS heterostructures [26–31].

Multiterminal hybrid structures consist of systems in which several spin polarized electrodes are connected to

[a] e-mail: melin@grenoble.cnrs.fr
[b] UPR 5001 du CNRS, Laboratoire conventionné avec l'Université Joseph Fourier

a superconductor and are controlled by crossed Andreev reflection processes in which the spin-up and spin-down electrons making the Cooper pair can tunnel in different ferromagnetic electrodes. Several theoretical predictions have been made. For instance the current circulating in one of the electrodes can be controlled by the voltage applied on another electrode [5,7]. The conductance can be described in terms of a conductance matrix [5] that can be calculated from Keldysh formalism [7]. Other predictions concern the proximity effect in FSF trilayers [32]. It was shown in reference [8] that the two ferromagnetic electrodes of the FSF trilayer are coupled by pair correlations and that the superconducting order parameter in the ferromagnetic alignment can be larger than the superconducting order parameter in the antiferromagnetic alignment ($\Delta_{\rm F} > \Delta_{\rm AF}$). One goal of our article is to find out the range of validity of this result and to bridge the gap with other predictions based on Usadel equations [32]. It was shown in the context of Usadel equations that the critical temperature (and therefore the superconducting order parameter) is larger in the antiferromagnetic alignment ($\Delta_{\rm AF} > \Delta_{\rm F}$) [32]. We show that the ballistic models that we consider can lead also to $\Delta_{\rm AF} > \Delta_{\rm F}$ if one takes into account the existence of a finite exchange field in the superconductor, in the spirit of reference [33]. There are thus two competing mechanisms for the proximity effect in FSF trilayers. The mechanism based on the exchange field involves the "11" and "22" diagonal elements of the Green's function of the superconductor connected to the ferromagnetic electrodes. The other mechanism based on pair correlations involves the "12" extra diagonal element. To understand in detail the mechanism based on pair correlations we investigate a device in which three ferromagnetic electrodes are coupled to a superconductor. As a simplifying assumption we suppose that the three electrodes are coupled to the same site in the superconductor. The fabrication of three contacts within a coherence length is not possible with present time state of the art technology. Nevertheless these systems with three electrodes provide idealized situations that are useful for understanding theoretically how the value of the superconducting order parameter depends on pair correlations induced in the ferromagnetic electrodes.

From the point of view of the method we use two complementary approaches: (i) an analytical evaluation of the high energy behavior of the Gorkov function; (ii) exact diagonalizations of the Bogoliubov-de Gennes equations. The analytical approach is based on the simplest ballistic models and can be a useful guideline for understanding more realistic systems in the future, such as multichannel systems or diffusive systems. An important difference between the analytical and numerical approaches lies in the fact that in the analytical calculation we suppose that the band-width of the superconductor is much larger than the superconducting gap like in realistic systems for which $\Delta/D \simeq 10^{-5}$. As a consequence of this assumption the integral appearing in the self-consistency relation is dominated by the high frequencies. By contrast in the numerical simulation the band-width of the superconductor is not small compared to the superconducting gap (typically the ratio between the bandwidth and the gap is $\Delta/D \simeq 1/5$). The analytical calculation and the numerical simulation correspond to different regimes and this is why all the analytical results cannot be confirmed by the numerical simulation. The numerical simulation is useful to discuss the behavior of the local density of states (LDOS), the case of a partial spin polarization and the spatial variation of the pair amplitude.

The article is organized as follows. Necessary technical preliminaries are given in Section 2. The mechanism based on the exchange field induced in the superconductor is investigated in Sections 3 and 4. The remaining of the article is devoted to the other mechanism based on pair correlations. In Section 5 we discuss the proximity effect in FSF heterostructures and generalize the results obtained in reference [8]. Namely we show that the superconducting order parameter is larger if the ferromagnetic electrodes have a parallel spin orientation. Multiterminal structures in which three electrodes are connected to a superconductor are discussed in Section 6. Friedel oscillations in the Gorkov function are analyzed in Section 7. Concluding remarks are given in Section 8.

2 Preliminaries

2.1 Green's function formalism

In this section we provide the technical details on Green's function formalism that is used throughout the article.

2.1.1 The models

The superconductor is described by a BCS lattice model

$$\mathcal{H}_{\rm BCS} = \sum_{\langle\alpha,\beta\rangle,\sigma} -t\left(c^+_{\alpha,\sigma}c_{\beta,\sigma} + c^+_{\beta,\sigma}c_{\alpha,\sigma}\right) + \sum_{\alpha}\left(\Delta_\alpha c^+_{\alpha,\uparrow}c^+_{\alpha,\downarrow} + \Delta^*_\alpha c_{\alpha,\downarrow}c_{\alpha,\uparrow}\right),$$

where Δ_α is the pairing interaction. The brackets indicate that hopping is between nearest neighbors. The ferromagnetic electrodes are described by a lattice Stoner model

$$\mathcal{H}_{\rm Stoner} = \sum_{\langle i,j\rangle,\sigma} -t\left(c^+_{i,\sigma}c_{j,\sigma} + c^+_{j,\sigma}c_{i,\sigma}\right) - h\sum_i\left(c^+_{i,\uparrow}c_{i,\uparrow} - c^+_{i,\downarrow}c_{i,\downarrow}\right),$$

where h is the exchange field. An exchange field smaller than the bandwidth corresponds to a partially polarized ferromagnet and an exchange field larger than the bandwidth corresponds to a half-metal ferromagnet in which only majority spins are present. We note ρ_0^S the normal state density of states of the superconductor and ρ_σ^F the spin-σ density of states in the ferromagnetic electrodes.

We use Greek symbols α, β, γ for the sites in the superconductor and Latin symbols a, b, c for the sites in the ferromagnetic electrodes. The tunnel Hamiltonian coupling the superconductor and the ferromagnetic electrodes takes the form

$$\hat{\mathcal{W}} = \sum_{k,\sigma} t_{a_k,\alpha_k} \left(c^+_{a_k,\sigma} c_{\alpha_k,\sigma} + c^+_{\alpha_k,\sigma} c_{a_k,\sigma} \right), \qquad (1)$$

where the sum over k runs over all contacts between the superconductor and the ferromagnetic electrodes.

2.1.2 Green's functions

The Green's functions of a connected system are obtained by solving the Dyson equation in the Nambu representation:

$$\hat{G}^{R,A} = \hat{g}^{R,A} + \hat{g}^{R,A} \otimes \hat{\Sigma} \otimes \hat{G}^{R,A}, \qquad (2)$$

where the self-energy $\hat{\Sigma}$ contains all couplings of the tunnel Hamiltonian given by (1). The Green's functions g correspond to the "disconnected" system in which $t_{a_k,\alpha_k} = 0$ (see Eq. (1)). The Dyson equation (2) is used to calculate the Green's functions of the connected system in which an electron in the superconductor can make excursions in the ferromagnetic electrodes.

We use the following notation for the Nambu representation of the advanced and retarded propagators of the disconnected system:

$$\hat{g}^{A,R}(t,t') = \begin{pmatrix} g^{A,R}(t,t') & f^{A,R}(t,t') \\ f^{A,R}(t,t') & g^{A,R}(t,t') \end{pmatrix},$$

with

$$g^A(t,t') = -\mathrm{i}\theta(t-t') \left\langle \left\{ c_{i,\uparrow}(t), c^+_{j,\uparrow}(t') \right\} \right\rangle \qquad (3)$$

$$f^A(t,t') = -\mathrm{i}\theta(t-t') \langle \{ c_{i,\uparrow}(t), c_{j,\downarrow}(t') \} \rangle, \qquad (4)$$

and we use the following notation for the Nambu representation of the density of states:

$$\hat{\rho} = \begin{pmatrix} \rho_g & \rho_f \\ \rho_f & \rho_g \end{pmatrix},$$

with $\rho_g = \frac{1}{\pi}\mathrm{Im}(g^A)$ and $\rho_f = \frac{1}{\pi}\mathrm{Im}(f^A)$. The Keldysh Green's function is obtained through the Dyson-Keldysh equation

$$\hat{G}^{+,-} = \left[\hat{I} + \hat{G}^R \otimes \hat{\Sigma} \right] \otimes \hat{g}^{+,-} \otimes \left[\hat{I} + \hat{\Sigma} \otimes \hat{G}^A \right], \qquad (5)$$

where $\hat{g}^{+,-}_{i,j} = 2\mathrm{i}\pi n_F(\omega - \mu_{i,j})\hat{\rho}_{i,j}$.

2.1.3 Superconducting order parameter and transport properties

In equilibrium the Keldysh Green's function defined by equation (5) simplifies into

$$\hat{G}^{+,-}_{\mathrm{eq}} = n_F(\omega - \mu_0) \left(\hat{G}^A - \hat{G}^R \right), \qquad (6)$$

where μ_0 is the chemical potential, identical in all conductors. The form (6) of the Keldysh Green's function at equilibrium can be used to obtain the superconducting order parameter in the superconductor *via* the self-consistency equation

$$\Delta_\beta = -U \int \frac{\mathrm{d}\omega}{2\mathrm{i}\pi} G^{+,-,1,2}_{\beta,\beta}(\omega). \qquad (7)$$

2.1.4 Green's function of an isolated normal metal

Evaluating the spectral representation for a normal metal leads to

$$g^A_{\alpha,\beta}(\omega) = -\frac{m a_0^2}{\hbar^2} \frac{a_0}{2\pi R_{\alpha,\beta}} \exp\left(-\mathrm{i}k_F R - \mathrm{i}\frac{\omega R_{\alpha,\beta}}{v_F} \right). \qquad (8)$$

The local density of states is given by

$$\rho_{\mathrm{loc}}(\omega) = \frac{1}{\pi}\mathrm{Im}\left[g^A(\omega) \right] = \frac{1}{2\pi^2} \frac{m a_0^3}{\hbar^2} \left(k_F + \frac{\omega}{v_F} \right). \qquad (9)$$

2.1.5 Green's function of an isolated insulator

We consider a semi-conductor model having a valence band at energy $\epsilon(k) = -\Delta - \hbar^2 k^2/(2m^*)$ and a conduction band at energy $\epsilon(k) = \Delta + \hbar^2 h^2/(2m^*)$. This model behaves like a band insulator if $|\omega| < \Delta$. The Green's functions in the energy range $|\omega| < \Delta$ are given by

$$g_{\alpha,\beta}(\omega) = \frac{m^* a_0^2}{\hbar^2} \frac{a_0}{2\pi R_{\alpha,\beta}} \left[\exp\left(-\frac{\sqrt{2m^* a_0^2}}{\hbar} \sqrt{\Delta + \omega} R \right) - \exp\left(-\frac{\sqrt{2m^* a_0^2}}{\hbar} \sqrt{\Delta - \omega} R \right) \right]. \qquad (10)$$

2.1.6 Green's functions of an isolated superconductor

The Green's function of an isolated superconductor with a uniform superconducting order parameter Δ_0 is obtained by evaluating the spectral representation [7]:

$$\hat{g}_{\alpha,\beta}(\omega) = \frac{2m a_0^2}{\hbar^2} \frac{a_0}{2\pi R} \exp\left[-\frac{R_{\alpha,\beta}}{\xi(\omega)} \right] \times \left\{ \frac{\sin\varphi_{\alpha,\beta}}{\sqrt{\Delta_0^2 - \omega^2}} \begin{bmatrix} -\omega & \Delta_0 \\ \Delta_0 & -\omega \end{bmatrix} + \cos\varphi_{\alpha,\beta} \begin{bmatrix} -1 & 0 \\ 0 & 1 \end{bmatrix} \right\}. \qquad (11)$$

Above the superconducting gap the retarded Green's function takes the form

$$\hat{g}^R_{\alpha,\beta} = \frac{2m a_0^2}{\hbar^2} \frac{a_0}{2\pi R} \exp\left[\mathrm{i}\frac{\sqrt{\omega^2 - \Delta_0^2} R_{\alpha,\beta}}{v_F} \right] \times \left\{ \frac{\mathrm{i}\sin\varphi_{\alpha,\beta}}{\sqrt{\omega^2 - \Delta_0^2}} \begin{bmatrix} -\omega & \Delta_0 \\ \Delta_0 & -\omega \end{bmatrix} + \cos\varphi_{\alpha,\beta} \begin{bmatrix} -1 & 0 \\ 0 & 1 \end{bmatrix} \right\}. \qquad (12)$$

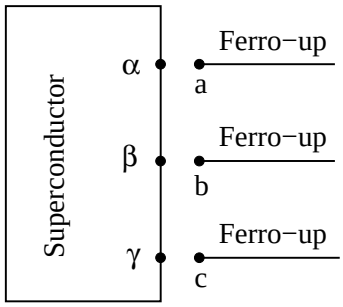

Fig. 1. Schematic representation of the model considered in Section 2.1.7 in which three half-metal ferromagnetic electrodes are connected to a superconductor.

The phase variable in equations (11) and (12) is $\varphi_{\alpha,\beta} = k_F R_{\alpha,\beta}$. The "local" propagators corresponding to $\alpha = \beta$ are described by $\varphi_{\alpha,\beta} = k_F R_0 = \pi/2$ [40]:

$$\hat{g}_{\rm loc}(\omega) = \frac{2ma_0^2}{\hbar^2}\frac{a_0}{2\pi R_0}\frac{1}{\sqrt{\Delta_0^2-\omega^2}}\begin{bmatrix} -\omega & \Delta_0 \\ \Delta_0 & -\omega \end{bmatrix}. \quad (13)$$

2.1.7 Dyson matrix

In this section we provide a derivation of the Dyson matrix in the simple case of three half-metal ferromagnetic electrodes connected to a superconductor (see Fig. 1). If λ is an arbitrary site in the superconductor, the Dyson equation (2) becomes

$$\hat{G}^{a_n,\lambda} = \begin{bmatrix} K_{1,1}^{a_n,\lambda} & K_{1,2}^{a_n,\lambda} \\ -K_{2,1}^{a_n,\lambda} & -K_{2,2}^{a_n,\lambda} \end{bmatrix} + \sum_m \begin{bmatrix} K_{1,1}^{a_n,\alpha_m} & -K_{1,2}^{a_n,\alpha_m} \\ -K_{2,1}^{a_n,\alpha_m} & K_{2,2}^{a_n,\alpha_m} \end{bmatrix} t_{\alpha_m,a_m}\hat{G}^{a_m,\lambda}, \quad (14)$$

with $K_{i,j}^{a_n,\alpha_m} = g_{i,i}^{a_n,a_n} t_{a_n,\alpha_n} g_{i,j}^{\alpha_n,\alpha_m}$, and

$$\hat{G}^{a_n,\lambda} = \begin{bmatrix} G_{1,1}^{a_n,\lambda} & G_{1,2}^{a_n,\lambda} \\ G_{2,1}^{a_n,\lambda} & G_{2,2}^{a_n,\lambda} \end{bmatrix}. \quad (15)$$

Equations (14, 15) are valid for an arbitrary spin polarization. In the case of the heterostructure in Figure 1 the explicit form of the Dyson matrix is the following:

$$\begin{bmatrix} 1-K_{1,1}^{a,\alpha}t_{\alpha,a} & -K_{1,1}^{a,\beta}t_{\beta,b} & -K_{1,1}^{a,\gamma}t_{\gamma,c} \\ -K_{1,1}^{b,\alpha}t_{\alpha,a} & 1-K_{1,1}^{b,\beta}t_{\beta,b} & -K_{1,1}^{b,\gamma}t_{\gamma,c} \\ -K_{1,1}^{c,\alpha}t_{\alpha,a} & -K_{1,1}^{c,\beta}t_{\beta,b} & 1-K_{1,1}^{c,\gamma}t_{\gamma,c} \end{bmatrix} \begin{bmatrix} G_{1,1}^{a,\lambda} \\ G_{1,1}^{b,\lambda} \\ G_{1,1}^{c,\lambda} \end{bmatrix} = \begin{bmatrix} K_{1,1}^{a,\lambda} \\ K_{1,1}^{b,\lambda} \\ K_{1,1}^{c,\lambda} \end{bmatrix}.$$

In Sections 4 we invert a similar form of the Dyson matrix in models involving four channels.

2.2 Exact diagonalizations of the Bogoliubov-de Gennes Hamiltonian

In the numerical simulations based on exact diagonalizations of the Bogoliubov-de Gennes Hamiltonian we use a lattice Hubbard model

$$\mathcal{H} = \sum_{\langle\alpha,\beta\rangle,\sigma} -t\left(c_{\alpha,\sigma}^+ c_{\beta,\sigma} + c_{\beta,\sigma}^+ c_{\alpha,\sigma}\right) + \mu\sum_{\alpha,\sigma} n_{\alpha,\sigma} + \sum_{\alpha,\sigma}\mu_\alpha^I n_{\alpha,\sigma} + \sum_{\alpha,\sigma} h_{\alpha,\sigma} n_{\alpha,\sigma} + V_0\sum_\alpha n_{\alpha,\uparrow} n_{\alpha,\downarrow}. \quad (16)$$

In equation (16) $n_{\alpha,\sigma} = c_{\alpha,\sigma}^+ c_{\alpha,\sigma}$ is the electron number operator at site α, μ is the chemical potential, $h_{\alpha,\sigma} = -h\sigma_z$ is the exchange field in the ferromagnetic region and $\sigma_z = \pm 1$ is the eigenvalue of the z component of the Pauli matrix. V_0 is the on-site interaction. We use negative values of V_0 corresponding to attractive interaction. To simulate the effect of depletion of the carrier density at the surface the site-dependent impurity potential μ_α^I is set to a sufficiently large value at the surface sites. This prohibits electron tunneling over these sites. Within a mean field approximation equation (16) reduces to the Bogoliubov-de Gennes equations [37,38]:

$$\begin{pmatrix} \hat{\xi} & \hat{\Delta} \\ \hat{\Delta}^* & -\hat{\xi} \end{pmatrix}\begin{pmatrix} u_{n,\uparrow}(r_\alpha) \\ v_{n,\downarrow}(r_\alpha) \end{pmatrix} = \epsilon_{n,\gamma_1}\begin{pmatrix} u_{n,\uparrow}(r_\alpha) \\ v_{n,\downarrow}(r_\alpha) \end{pmatrix}, \quad (17)$$

and

$$\begin{pmatrix} \hat{\xi} & \hat{\Delta} \\ \hat{\Delta}^* & -\hat{\xi} \end{pmatrix}\begin{pmatrix} u_{n,\downarrow}(r_\alpha) \\ v_{n,\uparrow}(r_\alpha) \end{pmatrix} = \epsilon_{n,\gamma_2}\begin{pmatrix} u_{n,\downarrow}(r_\alpha) \\ v_{n,\uparrow}(r_\alpha) \end{pmatrix}, \quad (18)$$

such that

$$\hat{\xi}u_{n,\sigma}(r_\alpha) = -t\sum_{\hat{\delta}} u_{n,\sigma}(r_\alpha+\hat{\delta}) + \left(\mu^I(r_\alpha)+\mu\right)u_{n,\sigma}(r_\alpha) + h_\alpha\sigma_z u_{n,\sigma}(r_\alpha) \quad (19)$$

$$\hat{\Delta}u_{n,\sigma}(r_\alpha) = \Delta_0(r_\alpha)u_{n,\sigma}(r_\alpha), \quad (20)$$

and where the pair potential is defined by

$$\Delta_0(r_\alpha) = V_0\left\langle c_\uparrow(r_\alpha)c_\downarrow(r_\alpha)\right\rangle.$$

In equation (19) $\hat{\delta} = \hat{x}, -\hat{x}, \hat{y}, -\hat{y}$ denotes the four directions of the square lattice. $\hat{\delta} = \hat{z}, -\hat{z}$ corresponds to the two directions in the ferromagnetic electrodes. The self-consistency equation takes the form

$$\Delta_0(r_\alpha) = \frac{V_0(r_\alpha)}{2}F(r_\alpha) = \frac{V_0(r_\alpha)}{2}\sum_n\left[u_{n,\uparrow}(r_\alpha)v_{v,\downarrow}^*(r_\alpha)\tanh\left(\frac{\beta\epsilon_{n,\gamma_1}}{2}\right) + u_{n,\downarrow}(r_\alpha)v_{n,\uparrow}^*(r_\alpha)\tanh\left(\frac{\beta\epsilon_{n,\gamma_2}}{2}\right)\right], \quad (21)$$

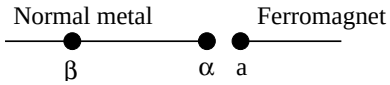

Fig. 2. Schematic representation of the single-channel junction between a normal metal and a ferromagnet. R is the distance between sites α and β.

where β is the inverse temperature. We start from an approximate solution for the gap profile $\Delta_0(r_\alpha)$. After exact diagonalizations of equations (17, 18) we obtain $u_{n,\sigma}(r_\alpha)$ and $v_{n,\sigma}(r_\alpha)$. The quasiparticle amplitudes are inserted into equation (21) and a new gap function is evaluated which is then inserted into equation (20) and we iterate until a sufficient precision has been obtained. Although the pair potential $\Delta_0(r_\alpha)$ is zero in the ferromagnet the pair amplitude $F(r_\alpha)$ is non zero. The LDOS at site α is given by

$$\rho_\alpha(E) = -\sum_{n,\sigma}\left[|u_{n,\sigma}(r_\alpha)|^2 f'(E-\epsilon_n) + |v_{n,\sigma}(r_\alpha)|^2 f'(E+\epsilon_n)\right], \quad (22)$$

where f' is the derivative of the Fermi function $f(\epsilon) = \frac{1}{1+\exp(\epsilon/k_BT)}$.

3 Friedel oscillations at a single NF interface

We start by considering a single interface between a normal metal and a spin polarized ferromagnet. We calculate the exchange field at site β in the normal metal, induced by the proximity of the ferromagnet (see Fig. 2). To order t^2 the Green's function at site β is given by

$$G_{\beta,\beta} = g_{\beta,\beta} + g_{\beta,\alpha}t_{\alpha,a}g_{a,a}t_{a,\alpha}g_{\alpha,\beta}. \quad (23)$$

$g^A_{\alpha,\beta}$ is given by equation (8) and $g^A_{a,a}$ is decomposed in a real and imaginary part: $g^A_{a,a} = g^{(R)}_{a,a} + \mathrm{i}g^{(I)}_{a,a}$. If the exchange field is small compared to the typical energy scales (being the energy band-width for a metal or the charge gap for an insulator) then the spin-up and spin-down Green's functions take the form

$$g^{(\sigma)}_{a,a}(\omega) = g^{(0)}_{a,a}(\omega) + \sigma h_{\rm ex}\frac{\partial g^{(0)}_{a,a}(\omega)}{\partial\omega},$$

where $g^{(0)}_{a,a}(\omega)$ is the Green's function in the absence of an exchange field. We deduce the existence of Friedel oscillations in the spin polarization at the Fermi surface:

$$P_\beta = \frac{\tilde\rho^{(\uparrow)}_{\beta,\beta} - \tilde\rho^{(\downarrow)}_{\beta,\beta}}{\tilde\rho^{(\uparrow)}_{\beta,\beta} + \tilde\rho^{(\downarrow)}_{\beta,\beta}} = 2\pi t_\alpha^2 \frac{1}{v_F}\left(\frac{1}{2\pi R}\right)^2 h_{\rm ex} \times\left[-\sin(2k_FR)\frac{\partial g^{(R)}_{a,a}}{\partial\omega}(0) + \cos(2k_FR)\frac{\partial g^{(I)}_{a,a}}{\partial\omega}(0)\right]. \quad (24)$$

For an insulating ferromagnet we obtain from equation (10) that $\partial g^{(R)}_{a,a}/\partial\omega(0)$ is negative which leads to a positive spin polarization at site α. For a metallic ferromagnet we obtain from equation (9) that $\partial g^{(I)}_{a,a}/\omega(0)$ is positive. Since we use $k_FR_0 = \pi/2$ we deduce that spin polarization at site α is negative. As far as the magnitude of the effective exchange field $h_{\rm eff}$ is concerned we see that $h_{\rm eff}$ is of order $(t_{a,\alpha}/\epsilon_F)^2 h_{\rm ex}$ in the metallic case and of order $t^2_{a,\alpha}\Delta^{-1/2}\left(m^*a_0^2/\hbar^2\right)^{3/2} h_{\rm ex}$ in the insulating model.

We note that in the insulating case the limit $R \to 0$ is well-defined and the value of spin polarization at site α does not depend on the value of the ultraviolet cut-off R_0 introduced at short length scale. In the metallic model the value of the spin polarization is diverging if one takes the limit $R \to 0$. Therefore the sign of spin polarization at site α depends on the value of the short distance cut-off R_0. In the analytical approaches we use a regularization in which we introduce a cut-off equal to $k_FR_0 = \pi/2$ that is chosen similarly to reference [40]. The justification of this choice of R_0 is that it leads to a physically acceptable value of the local density of states. The value of the density of states at the Fermi energy for $R = R_0$ is given by

$$\rho_{a,a}(R_0) = \frac{ma_0^2}{\hbar^2}\frac{a_0}{2\pi R_0}\sin(k_FR_0).$$

With the choice $k_FR_0 = \pi/2$ of the short distance cut-off the local density of state is equal to $\rho_{a,a}(R_0) = ma_0^3k_F/(\pi^2\hbar^2)$, a positive value that is not far from the exact density of states obtained for $R_0 = 0$ (see Eq. (9)).

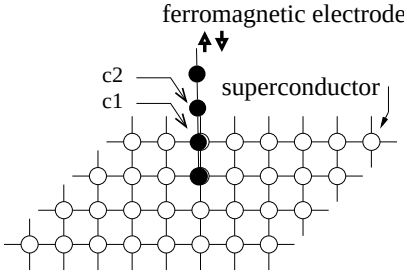

Fig. 3. The geometry used in the numerical simulations in Section 4. A one-dimensional ferromagnetic electrode is connected to a two-dimensional superconductor.

4 Proximity effect at a single FS interface

4.1 Local density of states

We first use exact diagonalizations of the Bogoliubov-de Gennes equations (see Sect. 2.2) to describe the proximity effect at a single FS interface. This constitutes a test of the numerical method and we recover some of the results for the LDOS obtained recently by means of a recursion method (see Ref. [36]).

We consider a two-dimensional superconducting system of 30×30 sites and we suppose fixed boundary conditions by setting the impurity potential $\mu^I = 100t$ at the surface. The temperature is $k_BT = 0.1t$ and the local attractive interaction in the superconducting region is $V_0 = -3.5t$. On top of the superconductor is attached a one-dimensional superconducting electrode of 50 sites (see Fig. 3). The transparency of the interface is controlled by changing the hopping element t_c connecting sites on both

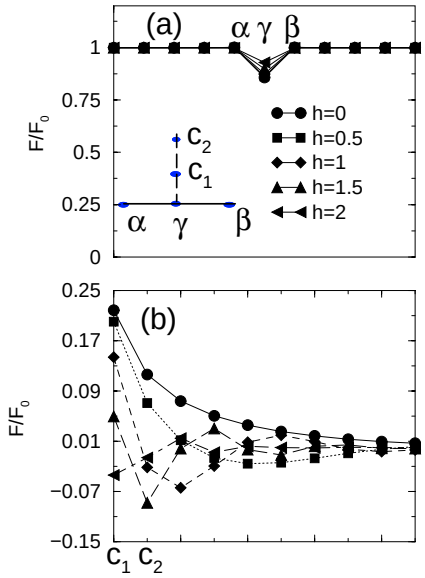

Fig. 4. (a) Pair amplitude for different values of the exchange field for several sites in the superconducting region at the interface of one-dimensional ferromagnetic electrode and a two-dimensional superconducting system. Sites α, γ, β belong to the superconductor while the sites c_1, c_2 belong to the ferromagnetic electrode. (b) Pair amplitude for several sites in the ferromagnetic region for different values of the exchange field. The pair amplitude in the superconductor does not vary much with the exchange field. The pair amplitude in the ferromagnetic electrode shows an oscillatory behavior. The pair amplitude decays monotonically in the absence of spin polarization in the ferromagnetic electrode.

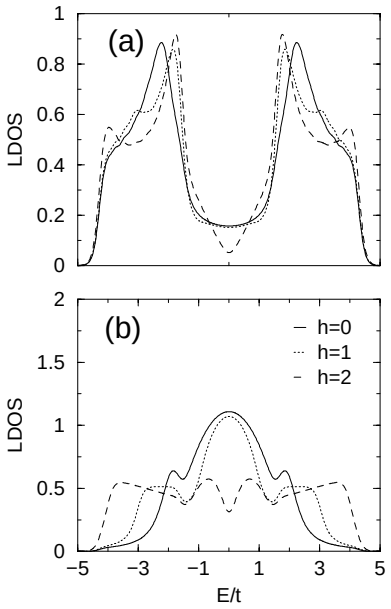

Fig. 5. (a) The LDOS at site γ in the superconductor for different values of the exchange field, for the geometry of Figure 4. (b) The LDOS at site c_1 in the ferromagnetic electrode for different values of the exchange field. The subgap LDOS is due to Andreev bound states.

sides of the interface and we restrict here to the case where the transparency of the interface is the same as inside the superconductor. In this case the pair amplitude in the superconducting system is not really modified as seen in Figure 4a while in the ferromagnetic region the pair amplitude oscillates around zero and the period of oscillations decreases with increasing the exchange field (see Fig. 4b). In the case of a zero exchange field the pair amplitude is decaying monotonically in the normal metal.

Due to the proximity effect the LDOS shows a gap structure even for the sites within the ferromagnet (see Fig. 5b). The conductance peaks within the gap are due to Andreev bound states [39] and have been discussed recently for a three dimensional FS interface using a recursion method [36]. The residual values of the LDOS are reduced by the increase of the exchange field. The Andreev bound states move towards the Fermi level and cross the Fermi level with increasing the exchange field.

4.2 Exchange field in the superconductor

From the discussion in Section 3 we deduce that a finite exchange field is induced in the superconductor [33]. The effect was also found in recent numerical simulations in reference [41]. In the metallic case and in the tunnel limit the magnitude of the exchange field is of order $(t_{a,\alpha}/\epsilon_F)^2 h_{\rm ex}$.

An exchange field in a superconductor is a pair-breaking perturbation that tends to dissociate Cooper pairs [37,42]. In this situation we expect that Cooper pairs couple to the exchange field averaged over a length scale equal to the BCS coherence length. A qualitative argument can be made from the NF model in Section 3. Since the discussion is similar in the two cases of metallic and insulating ferromagnets we consider a metallic ferromagnet model only. We obtain

$$\tilde{\rho}^{(\uparrow)}_{\beta,\beta}(\omega) - \tilde{\rho}^{(\downarrow)}_{\beta,\beta}(\omega) = \frac{t^2_{a,\alpha} h_{\rm ex}}{4\pi^4 k_F a_0} \left(\frac{m a_0^2}{\hbar^2}\right)^4 \times \left(\frac{a_0}{R}\right)^2 \cos\left[3(k_F + \omega/v_F)\right],$$

from what we deduce

$$\int_{R_0}^{+\infty} 4\pi R^2 {\rm d}R \int_0^D \left[\tilde{\rho}^{(\uparrow)}_{\beta,\beta}(\omega) - \tilde{\rho}^{(\downarrow)}_{\beta,\beta}(\omega)\right] {\rm d}\omega = - \frac{t^2_{a,\alpha} h_{\rm ex}}{3\pi^3} \left(\frac{m a_0^2}{\hbar^2}\right)^3 \int_{3k_F R_0}^{3\left(k_F + \frac{D}{v_F}\right) R_0} \frac{\sin u}{u} {\rm d}u.$$

With $k_F R_0 = \pi/2$ the spin polarization induced at long distance in the superconductor is positive but the local spin polarization at the contact is negative.

The reduction of the superconducting order parameter due to pair-breaking effects was observed in FSF trilayers with insulating ferromagnets in references [43,44]. The effect is not visible in the point contact experiments in reference [10] even though one might expect a reduction of the superconducting gap at the interface that would increase with increasing the exchange field. It is likely that

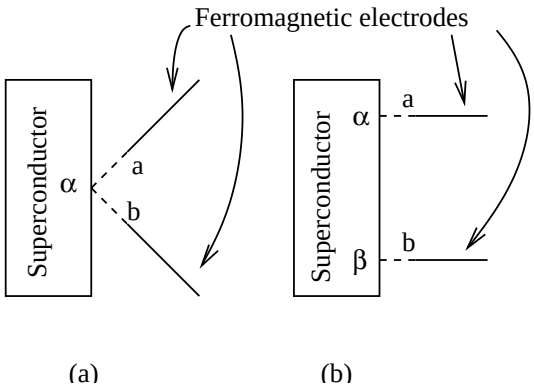

Fig. 6. The two models considered in Sections 5.2 and 7. In (a) the two ferromagnetic electrodes are connected to the same site in the superconductor. In (b) the two ferromagnetic electrodes are connected to two different sites in the superconductor. The two ferromagnetic electrodes contain a spin-up and a spin-down conduction band. The models are thus solved in a 4×4 formalism.

the point contact geometry used in reference [10] plays a role and that the effect should be more pronounced for extended contacts.

5 Proximity effect in FSF heterostructures: local models

Now we reconsider the proximity effect in a FSF heterostructure in which two ferromagnetic electrodes are connected to a superconductor. In this section as well as in Section 6 we consider "local" models in which two or three ferromagnetic electrodes are connected to the same site in the superconductor (see Figs. 6a and 7a).

5.1 Motivation

Two effects can play a role in the determination of the self-consistent order parameter:

(i) *The proximity effect* that takes place already at a single NS interface. A pair amplitude is generated in the normal metal and there is a reduction of the order parameter on the superconducting side of the interface [37, 42]. For the models in Figure 6 the two electrodes ending at sites "a" and "b" are coupled by pair correlations only in the antiferromagnetic alignment. The case of an antiparallel spin orientation is thus qualitatively similar to a NS interface in which case the order parameter in the superconductor is reduced at the interface. On the other hand no pair correlations are generated among the ferromagnetic electrodes in the parallel alignment if we consider half-metal ferromagnets. The case of parallel magnetization is thus similar to an isolated superconductor, from what we deduce that the superconducting order parameter is larger in the ferromagnetic alignment.

(ii) *Pair breaking effects* due the finite exchange field in the superconductor. The exchange field is a pair-breaking perturbation that tends to reduce the superconducting order parameter.

A relevant question is to determine which effect would control real experiments on metallic FSF trilayers. It is likely that the answer depends on the geometry of the devices. For small interface transparencies the exchange field in the superconductor is of order $(t/\epsilon_F)^2$ (see Sect. 4). For a thin film in a parallel field the pair breaking parameter is equal to $\alpha = De^2H^2d^2/(6\hbar c^2)$ with D the diffusion constant, H the magnetic field in tesla, d the width of the superconductor. The difference between the critical temperatures in the ferromagnetic and antiferromagnetic alignments is given by $k_B \Delta T_c = \pi\alpha/4$ [42] which is proportional to t^4 because H is proportional to t^2. On the other hand if the physics is dominated by the proximity effect we deduce from reference [6] that the difference between the superconducting order parameters in the ferromagnetic and antiferromagnetic alignments is of order $\Delta_{\rm F} - \Delta_{\rm AF} = t^4\Delta^{(0)}/(U\epsilon_F^3)$, with $\Delta^{(0)} = D\exp[-1/(U\rho_N)]$ the BCS superconducting order parameter. We see that ΔT_c due to pair-breaking effects is proportional to d^2 and we deduce that pair-breaking effects are reduced if the width of the superconducting layer is reduced.

In the following we focus on the effect of pair correlations induced in the ferromagnetic electrodes and we take for granted that the width of the superconductor is small enough so that pair-breaking effects can be neglected. We make the further simplifying assumption of considering that all ferromagnetic electrodes are connected to the same site and we calculate the superconducting order parameter at this site. The case of two electrodes at a finite distance will be considered in Section 7. The qualitative physics occurring in the schematic model with all electrodes connected to the same site can be described the following rule: *increasing pair correlations in the ferromagnetic electrodes tends to reduce the value of the self-consistent order parameter in the superconductor.*

To illustrate this let us first consider the case of two ferromagnetic electrodes connected to a superconductor (see Fig. 6a). Pair correlations among the two ferromagnets are stronger in the antiferromagnetic alignment than in the ferromagnetic alignment. As a consequence of the rule given above the superconducting order parameter is larger in the ferromagnetic alignment. To make a more refined test of this rule we consider in Section 6 a system in which three electrodes are connected to a superconductor (see Fig. 7a). For simplicity we consider that the three ferromagnetic electrodes are half-metal ferromagnets. Electrode c is supposed to have a spin-down orientation. Electrode a has a spin-up orientation. Electrode b can have a spin-up orientation (ferromagnetic alignment) or a spin-down orientation (antiferromagnetic alignment). If we consider first that $t_{c,\gamma}$ is small we see that pair correlations are formed mainly among electrodes a and b if electrodes a and b have an opposite spin orientation. We deduce that $\Delta_{\rm F} > \Delta_{\rm AF}$ if $t_{c,\gamma}$ is small. We consider now that $t_{c,\gamma}$ is large and electrode c has a spin-down

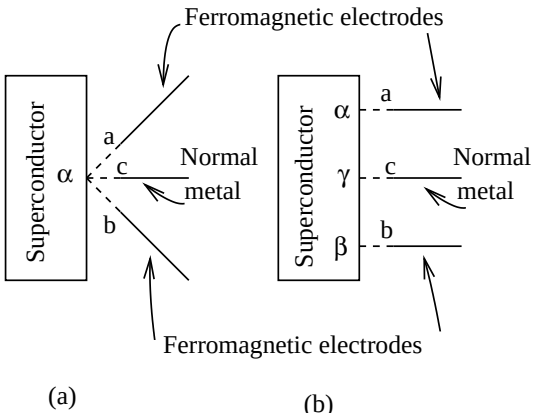

Fig. 7. The model considered in Section 6. In (a) the three electrodes are connected to the same site in the superconductor. In (b) the three electrodes are connected to two different sites in the superconductor. We use the model (a) to calculate the superconducting order parameter.

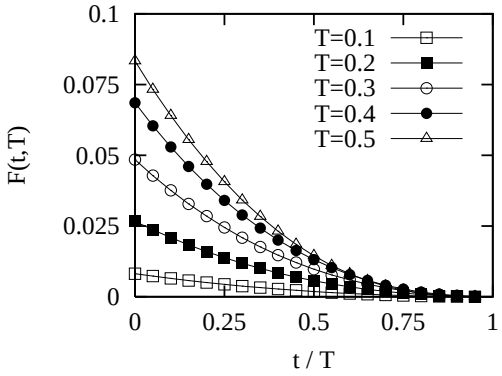

Fig. 8. Variation of $F(t,T)$ for different values of $T < 1/2$. We obtain $F(t,T) > 0$ which shows that the ferromagnetic superconducting order parameter is larger than the antiferromagnetic superconducting order parameter for large interface transparencies. The microscopic interaction U is such that the bulk superconducting gap is $\Delta_{\rm bulk} = 1$ and the bandwidth of the superconductor is $D = 100$.

orientation. If electrodes a and b have a spin-up orientation we see that pair correlations are formed mainly among electrode a and c and among electrodes b and c. If electrode a has a spin-up orientation and electrode b has a spin-down orientation we see that pair correlations are formed mainly among electrodes a and c. As a consequence the proximity effect is stronger if electrodes a and b have a parallel orientation. We deduce from the rule given above that $\Delta_{\rm F} < \Delta_{\rm AF}$ if $t_{c,\gamma}$ is large.

5.2 Two ferromagnetic electrodes connected to the same site

5.2.1 Sign of $\Delta_{\rm F} - \Delta_{\rm AF}$

Let us start with the situation where two ferromagnetic electrodes are connected to the same site (see Fig. 6a). We suppose that each ferromagnetic electrode is partially spin polarized and contains two spin channels. The model is thus solved in a 4×4 formalism. The Green's function $G^{A,1,2}_{\alpha,\alpha}$ is found to be

$$\begin{aligned} G^{A,1,2}_{\alpha,\alpha} = &-{\rm i}\pi\rho_0^S\frac{\Delta}{\omega} - {\rm i}\pi\rho_0^S\frac{\Delta}{\omega}\frac{1}{\mathcal{D}}\{-f(x_{a,\uparrow}) - f(x_{a,\downarrow}) \\ &- f(x_{b,\uparrow}) - f(x_{b,\downarrow}) + 2f(x_{a,\uparrow})f(x_{b,\uparrow}) + 2f(x_{a,\downarrow})f(x_{b,\downarrow}) \\ &+ f(x_{a,\uparrow})f(x_{a,\downarrow}) + f(x_{a,\uparrow})f(x_{b,\downarrow}) + f(x_{a,\downarrow})f(x_{b,\uparrow}) \\ &+ f(x_{b,\uparrow})f(x_{b,\downarrow}) - f(x_{a,\uparrow})f(x_{a,\downarrow})f(x_{b,\downarrow}) \\ &- f(x_{a,\uparrow})f(x_{a,\downarrow})f(x_{b,\uparrow}) - f(x_{a,\downarrow})f(x_{b,\uparrow})f(x_{b,\downarrow}) \\ &- f(x_{a,\uparrow})f(x_{b,\uparrow})f(x_{b,\downarrow}) - f(x_{a,\uparrow})f(x_{a,\downarrow})f(x_{b,\uparrow})f(x_{b,\downarrow})\}, \end{aligned} \tag{25}$$

with

$$\mathcal{D} = (1 - f(x_{a,\downarrow})f(x_{b,\downarrow}))\,(1 - f(x_{a,\uparrow})f(x_{b,\uparrow}))\,. \tag{26}$$

The interface transparencies are parametrized by $f(x_i) = x_i/(1+x_i)$, with $x_{a,\uparrow} = \pi^2 t^2_{a,\alpha}\rho^F_{a,\uparrow}\rho^S_0$, $x_{a,\downarrow} = \pi^2 t^2_{a,\alpha}\rho^F_{a,\downarrow}\rho^S_0$, $x_{b,\uparrow} = \pi^2 t^2_{b,\beta}\rho^F_{b,\uparrow}\rho^S_0$, $x_{b,\downarrow} = \pi^2 t^2_{b,\beta}\rho^F_{b,\downarrow}\rho^S_0$. The values of $f(x_i)$ are such that $0 < f(x_i) < 1/2$. We do not consider the regime $1/2 < f(x_i) < 1$ for which we find that the self-consistency relation is unstable.

We suppose that the two ferromagnets have an identical density of states and that the two contacts have identical transparencies. In the ferromagnetic alignment we use the notation $f(x_{a,\uparrow}) = f(x_{b,\uparrow}) = T$ and $f(x_{a,\downarrow}) = f(x_{b,\downarrow}) = t$. In the antiferromagnetic alignment we use the notation $f(x_{a,\uparrow}) = f(x_{b,\downarrow}) = T$ and $f(x_{a,\downarrow}) = f(x_{b,\uparrow}) = t$. To second order in T and t we obtain

$$G^{1,2,F}_{\alpha,\alpha} - G^{1,2,AF}_{\alpha,\alpha} = -{\rm i}\pi\rho_0^S\frac{\Delta}{\omega}(T-t)^2. \tag{27}$$

As a consequence in the regime of small interfaces transparencies we obtain $\Delta_{\rm F} > \Delta_{\rm AF}$. The regime of a large interface transparencies can be treated by evaluating numerically the difference between the Gorkov functions $G^{1,2,F}_{\alpha,\alpha} - G^{1,2,AF}_{\alpha,\alpha} = -{\rm i}\pi\rho_0^S\frac{\Delta}{\omega}F(T,t)$. It is visible in Figure 8 that $F(T,t)$ is positive for any value of $T < 1/2$ and $t < T$ so that the ferromagnetic superconducting order parameter is larger than the antiferromagnetic superconducting order parameter, in agreement with reference [8].

5.3 Local density of states and pair amplitude

We calculated the LDOS for a partial spin polarization by means of exact diagonalizations of the Bogoliubov-de Gennes Hamiltonian. The geometry of the simulation is represented in Figure 9. It is visible in Figure 10 that the low energy LDOS is larger in the ferromagnetic alignment than in the antiferromagnetic alignment.

The variation of the difference $F_{\rm F} - F_{\rm AF}$ between the pair amplitudes in the ferromagnetic and antiferromagnetic alignments as a function of the exchange field is

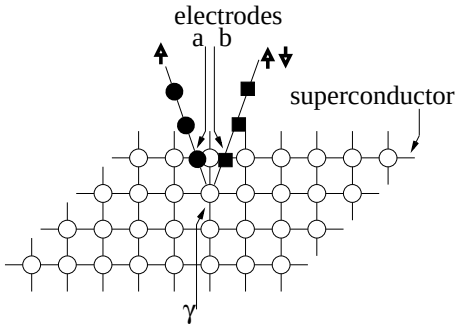

Fig. 9. The geometry used in the numerical simulations of the Bogoliubov-de Gennes Hamiltonian. Two one-dimensional ferromagnetic electrodes are connected to the same site of a two-dimensional superconductor. Electrode ending at site "a" is represented by filled circles and electrode ending at site "b" is represented by filled squares.

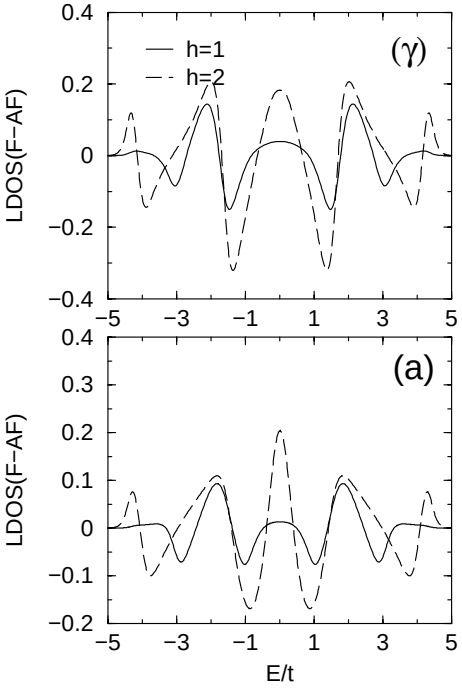

Fig. 10. Difference between the LDOS in the ferromagnetic and antiferromagnetic spin alignments for the geometry in Figure 9. The LDOS is represented as a function of E/t, for two values of the exchange field ($h = 1$ and $h = 2$). The upper panel corresponds to the LDOS at site γ and the lower panel corresponds to the LDOS at site a (see Fig. 9). The subgap LDOS is larger in the ferromagnetic alignment.

shown in Figure 11. The numerical simulation coincides with the analytical model for a large exchange field in the sense that the pair amplitude is larger in the ferromagnetic alignment. However for small values of the exchange field we obtain $F_{\rm F} > F_{\rm AF}$ or $F_{\rm F} < F_{\rm AF}$ depending on which lattice site is considered. The possible origin of the discrepancies between the numerical simulation and the analytical model are analyzed in the concluding section.

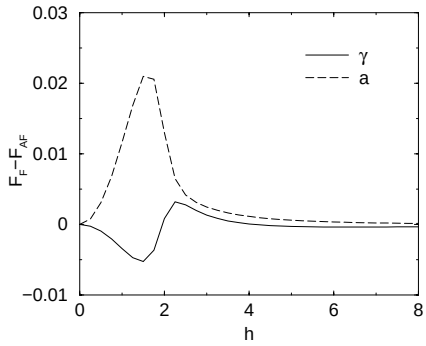

Fig. 11. The difference between the pair amplitudes in the ferromagnetic and antiferromagnetic alignments for two electrodes connected to the same site γ.

6 Proximity effect in multiterminal hybrid structures: local models

In this section we consider an heterostructure in which three electrodes are connected at the same site to a superconductor. Electrodes a and b in Figure 7 will be considered to be half-metal ferromagnets so that the models are solved in a 4×4 formalism. Using partially polarized ferromagnets would require to solve a 6×6 formalism for which we could not carry out the analytical calculation in the regime of large interface transparencies. The case of partially polarized ferromagnets will be treated numerically within exact diagonalizations of the Bogoliubov de Gennes equations.

6.1 Three electrodes connected at the same site

We consider a model in which three electrodes are connected to the same site α (see Fig. 7a). We determine the variation of $\Delta_{\rm F} - \Delta_{\rm AF}$ as a function of the transparency t_c of the contact with electrode c. We show that there is no change in the sign of $\Delta_{\rm F} - \Delta_{\rm AF}$ as t_c increases if electrode c is a normal metal. There is a change of sign in $\Delta_{\rm F} - \Delta_{\rm AF}$ as t_c increases if electrode c is a ferromagnet with a spin-down orientation. This is in agreement with the qualitative discussion in Section 5.1.

6.2 Sign of $\Delta_{\rm F} - \Delta_{\rm AF}$

In the ferromagnetic alignment the inversion of the 4×4 Dyson matrix leads to

$$G^{1,2}_{\alpha,\alpha} = -{\rm i}\pi\rho_0^S \frac{\Delta}{\omega} - {\rm i}\pi\rho_0^S \frac{\Delta}{\omega}\frac{1}{\mathcal{D}_{\rm F}}\{-f(x_a) - f(x_b) - f(x_{c,\uparrow})$$
$$- f(x_{c,\downarrow}) + 2f(x_a)f(x_b) + 2f(x_a)f(x_{c,\uparrow})$$
$$+ 2f(x_b)f(x_{c,\uparrow}) + f(x_a)f(x_{c,\downarrow}) + f(x_b)f(x_{c,\downarrow})$$
$$+ f(x_{c,\uparrow})f(x_{c,\downarrow}) - 3f(x_a)f(x_b)f(x_{c,\uparrow}) - f(x_a)f(x_b)f(x_{c,\downarrow})$$
$$- f(x_a)f(x_{c,\uparrow})f(x_{c,\downarrow}) - f(x_b)f(x_{c,\uparrow})f(x_{c,\downarrow})$$
$$+ f(x_a)f(x_b)f(x_{c,\uparrow})f(x_{c,\downarrow})\}, \quad (28)$$

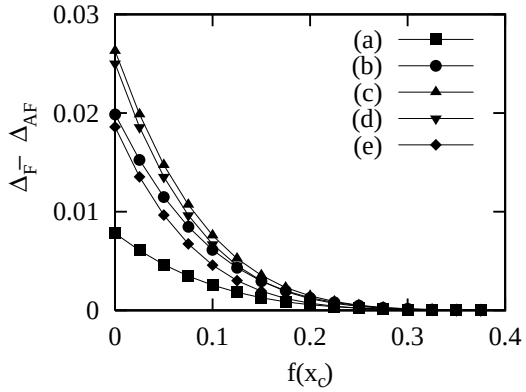

Fig. 12. Variation of $\Delta^F_{\alpha,\alpha} - \Delta^{AF}_{\alpha,\alpha}$ as a function of the transparency of the contact with the normal electrode $f(x_{c,\uparrow}) = f(x_{c,\downarrow})$ for different values of the transparency of the contacts with the ferromagnets $f(x_a) = f(x_b)$. The different curves correspond to (a) $f(x_a) = f(x_b) = 0.05$, (b) $f(x_a) = f(x_b) = 0.1$, (c) $f(x_a) = f(x_b) = 0.15$, (d) $f(x_a) = f(x_b) = 0.2$, (e) $f(x_a) = f(x_b) = 0.25$. We obtain $\Delta_{\rm F} > \Delta_{\rm AF}$. The microscopic interaction U is such that the superconducting order parameterof the isolated superconductor is $\Delta_{\rm bulk} = 1$ and the bandwidth of the superconductor is $D = 100$.

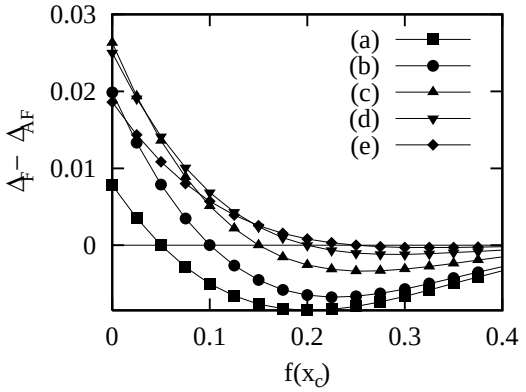

Fig. 13. Variation of $\Delta^F_{\alpha,\alpha} - \Delta^{AF}_{\alpha,\alpha}$ as a function of the transparency of the contact with the spin-down ferromagnetic electrode $f(x_{c,\downarrow})$ ($f(x_{c,\uparrow}) = 0$) for different values of the transparency of the contacts with the ferromagnets $f(x_a) = f(x_b)$. The different curves correspond to (a) $f(x_a) = f(x_b) = 0.05$, (b) $f(x_a) = f(x_b) = 0.1$, (c) $f(x_a) = f(x_b) = 0.15$, (d) $f(x_a) = f(x_b) = 0.2$, (e) $f(x_a) = f(x_b) = 0.25$. $\Delta_{\rm F} - \Delta_{\rm AF}$ changes sign as the transparency of the contact with electrode c increases. The microscopic interaction U is such that the superconducting order parameterof the isolated superconductor is $\Delta_{\rm bulk} = 1$ and the bandwidth of the superconductor is $D = 100$.

with

$$\mathcal{D}_{\rm F} = 1 - f(x_a)f(x_b) - f(x_a)f(x_{c,\uparrow}) - f(x_b)f(x_{c,\uparrow}) + 2f(x_a)f(x_b)f(x_{c,\uparrow}).$$

In the antiferromagnetic alignment we find

$$\begin{aligned} G^{1,2}_{\alpha,\alpha} = &-{\rm i}\pi\rho_0^S\frac{\Delta}{\omega} - {\rm i}\pi\rho_0^S\frac{\Delta}{\omega}\frac{1}{\mathcal{D}_{\rm AF}}\{-f(x_a) - f(x_b) \\ &- f(x_{c,\uparrow}) - f(x_{c,\downarrow}) + 2f(x_a)f(x_{c,\uparrow}) + 2f(x_b)f(x_{c,\downarrow}) \\ &+ f(x_a)f(x_b) + f(x_a)f(x_{c,\downarrow}) + f(x_b)f(x_{c,\uparrow}) \\ &+ f(x_{c,\uparrow})f(x_{c,\downarrow}) - f(x_a)f(x_b)f(x_{c,\downarrow}) \\ &- f(x_a)f(x_b)f(x_{c,\uparrow}) - f(x_b)f(x_{c,\uparrow})f(x_{c,\downarrow}) \\ &- f(x_a)f(x_{c,\uparrow})f(x_{c,\downarrow}) - f(x_a)f(x_b)f(x_{c,\uparrow})f(x_{c,\downarrow})\}, \end{aligned} \tag{29}$$

with

$$\mathcal{D}_{\rm AF} = 1 - f(x_b)f(x_{c,\downarrow}) - f(x_a)f(x_{c,\uparrow}) + f(x_a)f(x_b)f(x_{c,\uparrow})f(x_{c,\downarrow}).$$

The variation of $\Delta^F_{\alpha,\alpha} - \Delta^{AF}_{\alpha,\alpha}$ as a function of the transparency of the contact with electrode c is shown in Figure 12. It is visible on this figure that $\Delta_{\rm F} > \Delta_{\rm AF}$ for all values of the transparency $f(x_c)$ with interface c.

We also evaluated $\Delta_{\rm F} - \Delta_{\rm AF}$ in the case where electrode c is a half-metal ferromagnet with a spin-down orientation. We obtain a change of sign in $\Delta^F_{\alpha,\alpha} - \Delta^{AF}_{\alpha,\alpha}$ as the transparency of the interface with the ferromagnetic electrode c is increased (see Fig. 13). This change of sign can be described by expanding the Gorkov functions to second order in $f(x_a)$ and $f(x_b)$:

$$\begin{aligned} G^{1,2,{\rm Ferro}}_{\alpha,\alpha} = &-{\rm i}\pi\rho_0^S\frac{\Delta}{\omega} - {\rm i}\pi\rho_0^S\frac{\Delta}{\omega}[-f(x_a) - f(x_b) - f(x_{c,\uparrow}) \\ &- f(x_{c,\downarrow}) + 2f(x_a)f(x_b) + 2f(x_a)f(x_{c,\uparrow}) \\ &+ 2f(x_b)f(x_{c,\uparrow}) + f(x_a)f(x_{c,\downarrow}) \\ &+ f(x_b)f(x_{c,\downarrow}) + f(x_{c,\uparrow})f(x_{c,\downarrow})] \end{aligned} \tag{30}$$

$$\begin{aligned} G^{1,2,{\rm Antiferro}}_{\alpha,\alpha} = &-{\rm i}\pi\rho_0^S\frac{\Delta}{\omega} - {\rm i}\pi\rho_0^S\frac{\Delta}{\omega}[-f(x_a) - f(x_b) - f(x_{c,\uparrow}) \\ &- f(x_{c,\downarrow}) + 2f(x_a)f(x_{c,\uparrow}) + 2f(x_b)f(x_{c,\downarrow}) \\ &+ f(x_a)f(x_b) + f(x_a)f(x_{c,\downarrow}) + f(x_b)f(x_{c,\uparrow}) \\ &+ f(x_{c,\uparrow})f(x_{c,\downarrow})], \end{aligned} \tag{31}$$

from what we deduce that the difference between the ferromagnetic and antiferromagnetic superconducting order parameters changes sign if $f(x_{c,\downarrow}) = f(x_a) + f(x_{c,\uparrow})$, in agreement with Figure 13.

6.3 Three node circuit model

The presence or absence of sign changes in $\Delta^F_{\alpha,\alpha} - \Delta^{AF}_{\alpha,\alpha}$ discussed in Section 6.2 can also be obtained in the framework of a phenomenological circuit model [6]. In this model the superconducting order parameter is given by

$$\Delta = D\exp\left[-\frac{1}{U\rho_N}\left(1 + \pi\rho_N\Gamma_\uparrow\right)\left(1 + \pi\rho_N\Gamma_\downarrow\right)\right],$$

where ρ_N is the density of states in the normal state, and where Γ_σ is the total spectral line-width of spin-σ electrons, obtained as the sum of the spectral line-widths associated to each electrode [6]:

$$\Gamma_\sigma = \sum_k |t_{S,\alpha_k}|^2 \rho_{k,\sigma},$$

where t_{S,α_k} is the tunnel amplitude connecting the superconductor and the ferromagnetic electrode α_k.

Electrodes a and b are supposed to have the same spin polarization. We denote by $\gamma = |t_{S,a}|^2 \rho_{a,\uparrow}$ the spectral line-width associated to majority-spin electrons in electrode a and by $\lambda\gamma = |t_{S,a}|^2 \rho_{a,\downarrow}$ the spectral line-width associated to minority-spin electrons in electrode a. The spin polarization of the ferromagnetic electrodes is $P = (1-\lambda)/(1+\lambda)$.

We first suppose that electrode c is a ferromagnet having a spin-down orientation with a spectral line-width γ_0 associated to majority-spin electrons and a spectral line-width $\lambda\gamma_0$ associated to minority-spin electrons. If the ferromagnets a and b have a parallel spin orientation the total spectral line-widths are given by $\Gamma_\uparrow = 2\gamma + \lambda\gamma_0$ and $\Gamma_\downarrow = 2\lambda\gamma + \gamma_0$. If the ferromagnets a and b have an antiparallel spin orientation the total spectral line-widths are given by $\Gamma_\uparrow = (1+\lambda)\gamma + \lambda\gamma_0$ and $\Gamma_\downarrow = (1+\lambda)\gamma + \gamma_0$. We obtain

$$\frac{\Delta_{\rm F}}{\Delta_{\rm AF}} = \exp\left[\frac{\pi^2\rho_N}{U}(1-\lambda)^2\left(\gamma^2 - \gamma_0^2\right)\right],$$

from what we deduce that $\Delta_{\rm F} > \Delta_{\rm AF}$ if $\gamma_0 < \gamma$ and $\Delta_{\rm F} < \Delta_{\rm AF}$ if $\gamma_0 > \gamma$, in agreement with the microscopic model discussed in Section 6.2. A similar calculation in the case where electrode c is a spin-up ferromagnet shows that there is no sign change in $\Delta_{\rm F} - \Delta_{\rm AF}$.

The presence of a sign change in $\Delta_{\rm F} - \Delta_{\rm AF}$ as γ increases was anticipated in Section 5.1. The value $\gamma = \gamma_0$ at which the change of sign takes place can be understood from the following symmetry argument. In the ferromagnetic alignment of electrodes a and b, electrodes a and b have a spin-up orientation and electrode c has a spin-down orientation. In the antiferromagnetic alignment electrode a has a spin-up orientation and electrodes b and c have a spin-down orientation. Therefore if the three contacts have the same transparency (namely if $\gamma = \gamma_0$) we see that the case of a ferromagnetic alignment of electrode a and b can be deduced from the case of an antiferromagnetic alignment just by reversing the spin of the three ferromagnetic electrodes. As a consequence we obtain $\Delta_{\rm F} - \Delta_{\rm AF} = 0$ if $\gamma = \gamma_0$ and therefore a sign change in $\Delta_{\rm F} - \Delta_{\rm AF}$ if $\gamma = \gamma_0$. This argument is also in agreement with the fact that $\Delta_{\rm F} - \Delta_{\rm AF}$ changes sign for $f(x_c) = f(x_a) = f(x_b)$ in the microscopic model in which three electrodes are connected to the same site (see Fig. 13).

We suppose now that electrode c is a normal metal with a spectral line-width γ_0 associated to spin-up and spin-down electrons. We obtain

$$\frac{\Delta_{\rm F}}{\Delta_{\rm AF}} = \exp\left[\frac{\pi^2\rho_N}{U}(1-\lambda)^2\gamma^2\right]$$

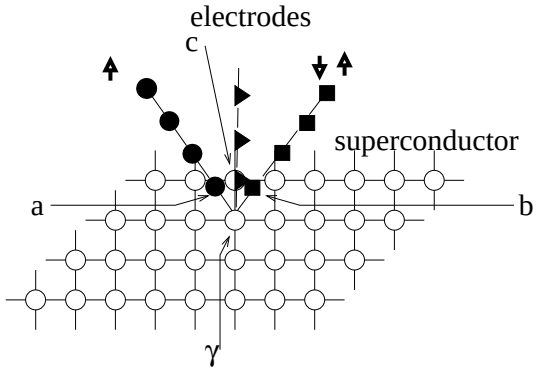

Fig. 14. The geometry used in the numerical simulation in which three one-dimensional electrodes are connected to a two-dimensional superconductor. Electrode ending at site "a" is ferromagnetic and is represented by filled circles. Electrode ending at site "b" is ferromagnetic and is represented by filled squares. Electrode ending at site "c" is a normal metal and is represented by filled triangles.

which leads to $\Delta_{\rm F} > \Delta_{\rm AF}$ for all values of γ_0, in agreement with Section 6.2.

6.4 Diagonalizations of the Bogoliubov-de Gennes Hamiltonian

We consider exact diagonalizations of the Bogoliubov-de Gennes Hamiltonian in a situation where a two-dimensional superconducting system is connected to two one-dimensional ferromagnetic electrodes and to a one-dimensional normal metal electrode (see Fig. 14). The proximity effect in the normal metal electrode can be controlled by the spin orientation of the two ferromagnetic electrodes in the sense that the LDOS in the normal metal electrode depends on the relative spin orientation of the ferromagnetic electrodes.

The LDOS at site c is shown in Figures 15a and b in the cases of antiparallel and parallel spin orientation of electrodes a and b. It is visible that for a sufficiently large exchange field the LDOS in the normal metal electrode depends on the relative spin orientation of the ferromagnetic electrodes. As a consequence it may be possible to control the proximity effect in the normal metal by changing the spin orientation of the ferromagnetic electrodes. This may be of interest in view of STM experiments similar to reference [46].

7 Friedel oscillations in the Gorkov function

Sections 5 and 6 were devoted to the analysis of "local" models in which several electrodes are connected to the same site in the superconductor. Now we consider the same problem but with a finite distance between the ferromagnetic electrodes. As discussed in Section 5.1 we suppose that the width of the superconductor is small enough so that pair-breaking effects due to the finite exchange

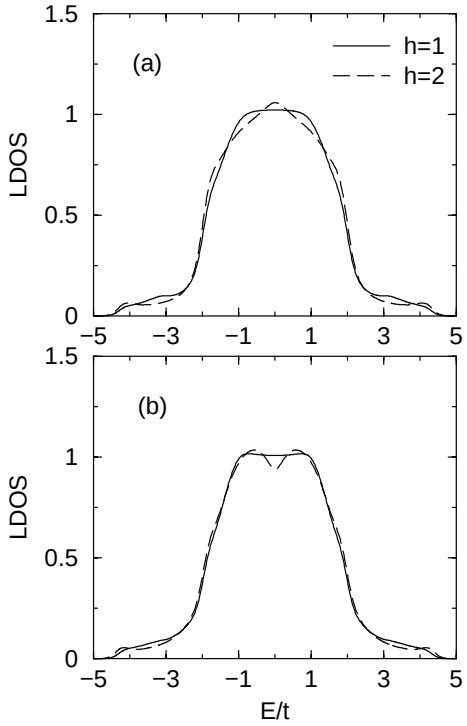

Fig. 15. (a) The LDOS as a function of E/t at the interface of a multiterminal junction made of two one-dimensional ferromagnetic electrodes and a one-dimensional normal metal electrode that are connected on top of a two dimensional superconducting system. The LDOS is calculated at site c in the normal metal electrode. The upper panel corresponds to the antiferromagnetic alignment and the lower panel corresponds to the ferromagnetic alignment.

field can be disregarded. We consider the geometry in Figure 6 in which a superconductor is in contact with two ferromagnetic electrodes a and a'. Compared to Figure 6 we use the notation α' and a' rather than β and b for the second electrode. We keep the notation β for an arbitrary site in the superconductor at which we calculate the superconducting order parameter. We suppose that the two electrodes a and a' are at a distance much larger than the Fermi wave-length.

7.1 Form of the Gorkov function

Electrodes a and a' are characterized by the microscopic propagators $\hat{g}_{a,a}$ and $\hat{g}_{a',a'}$. To order t^4 the Green's function at site β is given by

$$\begin{aligned}\hat{G}_{\beta,\beta} &= \hat{g}_{\beta,\beta} + \hat{g}_{\beta,\alpha}\hat{t}_{\alpha,a}\hat{g}_{a,a}\hat{t}_{a,\alpha}\hat{g}_{\alpha,\beta} \\ &+ \hat{g}_{\beta,\alpha'}\hat{t}_{\alpha',a'}\hat{g}_{a',a'}\hat{t}_{a',\alpha'}\hat{g}_{\alpha',\beta} && (32)\\ &+ \hat{g}_{\beta,\alpha}\hat{t}_{\alpha,a}\hat{g}_{a,a}\hat{t}_{a,\alpha}\hat{g}_{\alpha,\alpha}\hat{t}_{\alpha,a}\hat{g}_{a,a}\hat{t}_{a,\alpha}\hat{g}_{\alpha,\beta} && (33)\\ &+ \hat{g}_{\beta,\alpha}\hat{t}_{\alpha,a}\hat{g}_{a,a}\hat{t}_{a,\alpha}\hat{g}_{\alpha,\alpha'}\hat{t}_{\alpha',a'}\hat{g}_{a',a'}\hat{t}_{a',\alpha'}\hat{g}_{\alpha',\beta} && (34)\\ &+ \hat{g}_{\beta,\alpha'}\hat{t}_{\alpha',a'}\hat{g}_{a',a'}\hat{t}_{a',\alpha'}\hat{g}_{\alpha',\alpha}\hat{t}_{\alpha,a}\hat{g}_{a,a}\hat{t}_{a,\alpha}\hat{g}_{\alpha,\beta} && (35)\\ &+ \hat{g}_{\beta,\alpha'}\hat{t}_{\alpha',a'}\hat{g}_{a',a'}\hat{t}_{a',\alpha'}\hat{g}_{\alpha',\alpha'}\hat{t}_{\alpha',a'}\hat{g}_{a',a'}\hat{t}_{a',\alpha'}\hat{g}_{\alpha',\beta}. && (36)\end{aligned}$$

To lowest order the information about the exchange field in the superconductor is contained in the "11" and "22" components of the two terms in equation (32). The "12" component of the two terms in equation (32) contains the information about the effect of a single interface on the Gorkov function at order t^2. The two terms in equations (33) and (36) describe a single interface to order t^4 and are not directly relevant to our discussion since they are just a small correction of the terms in equation (32) obtained at order t^2. The "12" component of the two terms (34) and (35) describe the modification of the Gorkov function due to processes coupling the two interfaces. Each of the two terms (34) and (35) gives rise to three terms in the Gorkov function when the summation over spin indexes is made explicit:

$$\begin{aligned}(34) &= \hat{g}^{1,2}_{\beta,\alpha}t_{\alpha,a}\hat{g}^{2,2}_{a,a}t_{a,\alpha}\hat{g}^{2,2}_{\alpha,\alpha'}t_{\alpha',a'}\hat{g}^{2,2}_{a',a'}t_{a',\alpha'}\hat{g}^{2,2}_{\alpha',\beta} && (37)\\ &+ \hat{g}^{1,1}_{\beta,\alpha}t_{\alpha,a}\hat{g}^{1,1}_{a,a}t_{a,\alpha}\hat{g}^{1,2}_{\alpha,\alpha'}t_{\alpha',a'}\hat{g}^{2,2}_{a',a'}t_{a',\alpha'}\hat{g}^{2,2}_{\alpha',\beta} && (38)\\ &+ \hat{g}^{1,1}_{\beta,\alpha}t_{\alpha,a}\hat{g}^{1,1}_{a,a}t_{a,\alpha}\hat{g}^{1,1}_{\alpha,\alpha'}t_{\alpha',a'}\hat{g}^{1,1}_{a',a'}t_{a',\alpha'}\hat{g}^{1,2}_{\alpha',\beta} && (39)\\ (35) &= \hat{g}^{1,2}_{\beta,\alpha'}t_{\alpha',a'}\hat{g}^{2,2}_{a',a'}t_{a',\alpha'}\hat{g}^{2,2}_{\alpha',\alpha}t_{\alpha,a}\hat{g}^{2,2}_{a,a}t_{a,\alpha}\hat{g}^{2,2}_{\alpha,\beta} && (40)\\ &+ \hat{g}^{1,1}_{\beta,\alpha'}t_{\alpha',a'}\hat{g}^{1,1}_{a',a'}t_{a',\alpha'}\hat{g}^{1,2}_{\alpha',\alpha}t_{\alpha,a}\hat{g}^{2,2}_{a,a}t_{a,\alpha}\hat{g}^{2,2}_{\alpha,\beta} && (41)\\ &+ \hat{g}^{1,1}_{\beta,\alpha'_k}t_{\alpha',a'}\hat{g}^{1,1}_{a',a'}t_{a',\alpha'}\hat{g}^{1,1}_{\alpha',\alpha}t_{\alpha,a}\hat{g}^{1,1}_{a,a}t_{a,\alpha}\hat{g}^{1,2}_{\alpha,\beta}. && (42)\end{aligned}$$

7.2 Friedel oscillations in the Gorkov function

Now we use a single channel model to discuss Friedel oscillations in the Gorkov function. The terms of order t^2 are discussed in Section 7.2.1 and the terms of order t^4 are discussed in Section 7.2.2.

7.2.1 Terms of order t^2

Let us start with the terms of order t^2. Since these terms do not couple the two interfaces we consider a single interface only. We obtain easily the expression of the Gorkov function to order t^2:

$$G^{1,2,A}_{\beta,\beta} = -\mathrm{i}\frac{2ma_0^2}{\hbar^2}\frac{a_0}{2\pi R_0}\frac{\Delta}{\sqrt{\omega^2-\Delta^2}} \qquad (43)$$

$$\begin{aligned}&-\left(\frac{2ma_0^2}{\hbar^2}\right)^2\left(\frac{a_0}{2\pi R}\right)^2\pi t_\alpha^2\left[\rho_{a,\uparrow}\mathrm{e}^{-\mathrm{i}k_FR}-\rho_{a,\downarrow}\mathrm{e}^{\mathrm{i}k_FR}\right]\\ &\times\sin\left[k_FR\right]\exp\left[-\frac{2\mathrm{i}\sqrt{\omega^2-\Delta^2}R}{v_F}\right]\frac{\Delta}{\sqrt{\omega^2-\Delta^2}}\,. \qquad (44)\end{aligned}$$

If site β is equal to site α we use the regularization $k_FR_0 = \pi/2$ discussed in Section 3 to obtain the self-consistent

$$G(R) = \frac{1}{R_{\alpha,\beta}R_{\alpha,\alpha'}R_{\alpha',\beta}} \times \left\{ 2\rho_{a,\uparrow}\rho_{a',\downarrow} \int_{\Delta}^{D} \mathrm{d}\omega \frac{\Delta}{\sqrt{\omega^2-\Delta^2}} \sin\left\{ \left[k_F - \frac{\omega^2-\Delta^2}{v_F} \right] \left[R_{\alpha,\beta} + R_{\alpha,\alpha'} + R_{\alpha',\beta} \right] \right\} \right. \quad (47)$$

$$+ 2\rho_{a,\uparrow}\rho_{a',\uparrow} \int_{\Delta}^{D} \mathrm{d}\omega \frac{\Delta}{\sqrt{\omega^2-\Delta^2}} \sin\left\{ \left[k_F + \frac{\sqrt{\omega^2-\Delta^2}}{v_F} \right] \left[R_{\alpha,\beta} + R_{\alpha,\alpha'} + R_{\alpha',\beta} \right] \right\} \quad (48)$$

$$+ \left(\rho_{a,\uparrow} + \rho_{a,\downarrow}\right) \rho_{a',\downarrow} \int_{\Delta}^{D} \mathrm{d}\omega \frac{\Delta}{\sqrt{\omega^2-\Delta^2}} \sin\left\{ \left[k_F + \frac{\sqrt{\omega^2-\Delta^2}}{v_F} \right] R_{\alpha,\beta} - \left[k_F - \frac{\sqrt{\omega^2-\Delta^2}}{v_F} \right] \left[R_{\alpha,\alpha'} + R_{\alpha',\beta} \right] \right\} \quad (49)$$

$$+ \left(\rho_{a,\uparrow} + \rho_{a,\downarrow}\right) \rho_{a',\uparrow} \int_{\Delta}^{D} \mathrm{d}\omega \frac{\Delta}{\sqrt{\omega^2-\Delta^2}} \sin\left\{ \left[k_F - \frac{\sqrt{\omega^2-\Delta^2}}{v_F} \right] R_{\alpha,\beta} - \left[k_F + \frac{\sqrt{\omega^2-\Delta^2}}{v_F} \right] \left[R_{\alpha,\alpha'} + R_{\alpha',\beta} \right] \right\} \quad (50)$$

$$+ \rho_{a,\uparrow} \left(\rho_{a',\uparrow} + \rho_{a',\downarrow}\right) \int_{\Delta}^{D} \mathrm{d}\omega \frac{\Delta}{\sqrt{\omega^2-\Delta^2}} \sin\left\{ - \left[k_F + \frac{\sqrt{\omega^2-\Delta^2}}{v_F} \right] \left[R_{\alpha,\beta} + R_{\alpha,\alpha'} \right] + \left[k_F - \frac{\sqrt{\omega^2-\Delta^2}}{v_F} \right] R_{\alpha',\beta} \right\} \quad (51)$$

$$+ \left. \rho_{a,\downarrow} \left(\rho_{a',\uparrow} + \rho_{a',\downarrow}\right) \int_{\Delta}^{D} \mathrm{d}\omega \frac{\Delta}{\sqrt{\omega^2-\Delta^2}} \sin\left\{ - \left[k_F - \frac{\sqrt{\omega^2-\Delta^2}}{v_F} \right] \left[R_{\alpha,\beta} + R_{\alpha,\alpha'} \right] + \left[k_F + \frac{\sqrt{\omega^2-\Delta^2}}{v_F} \right] R_{\alpha',\beta} \right\} \right\}. \quad (52)$$

order parameter at the interface:

$$\Delta_\alpha = 2D \exp\left[-\frac{1}{U} \left\{ \frac{2ma_0^2}{\pi\hbar^2} \frac{a_0}{2\pi R_0} \times \left[1 - \frac{2ma_0^2}{\hbar^2} \frac{a_0}{2\pi R_0} \pi t_\alpha^2 \left(\rho_{a,\uparrow} + \rho_{a,\downarrow}\right) \right] \right\}^{-1} \right].$$

As expected the superconducting order parameter at the interface is reduced because of the proximity effect.

To discuss the proximity effect in the bulk of the superconductor we write the pair amplitude under the form

$$\int_{\Delta}^{D} \mathrm{Im}\left[G_{\beta,\beta}^{1,2,A} \right] \mathrm{d}\omega = -\frac{2ma_0^2}{\hbar^2} \frac{a_0}{2\pi R_0} \int_{\Delta}^{D} \frac{\Delta}{\sqrt{\omega^2-\Delta^2}} \mathrm{d}\omega + \left(\frac{2ma_0^2}{\hbar^2} \right)^2 \left(\frac{a_0}{2\pi} \right)^2 \pi t_\alpha^2 F(R),$$

with

$$F(R) = \frac{\sin\left[k_F R\right]}{R^2} \int_{\Delta}^{D} \left[\rho_{a,\uparrow} \sin\left\{ \left[k_F + \frac{2\sqrt{\omega^2-\Delta^2}}{v_F} R \right] \right\} + \rho_{a,\downarrow} \sin\left\{ \left[k_F - \frac{2\sqrt{\omega^2-\Delta^2}}{v_F} R \right] \right\} \right] \frac{\Delta}{\sqrt{\omega^2-\Delta^2}} \mathrm{d}\omega. \quad (45)$$

The variations of $F(R)$ as a function of R are shown in Figure 16. It is visible that $F(R)$ oscillates in space but is always positive which means that the superconducting order parameter is reduced in the bulk of the superconductor and shows Friedel oscillations.

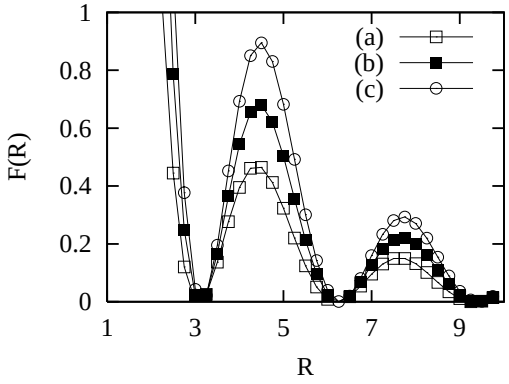

Fig. 16. Variation of $F(R)$ defined by equation (45). We used the parameters $k_F = 1$, $\Delta = 1$, $D = 10^5$ and $v_F = D/k_F$. The spin-up density of states is $\rho_{a,\uparrow} = 1$. The spin-down density of states is $\rho_{a,\downarrow} = 0$ (a), $\rho_{a,\downarrow} = 0.5$ (b) and $\rho_{a,\downarrow} = 1$ (c).

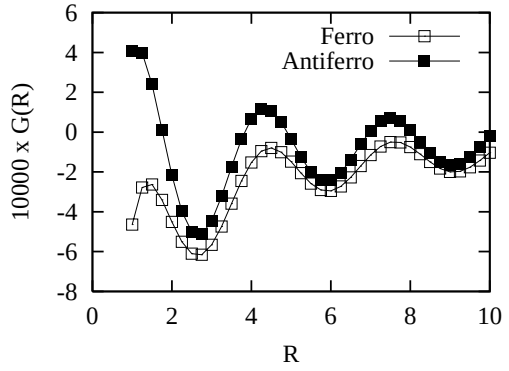

Fig. 17. Variation of $G(R)$ defined by equation (47). We used the parameters $k_F = 1$, $\Delta = 1$, $D = 10^5$ and $v_F = D/k_F$. The spin-up density of states is $\rho_{a,\uparrow} = 1$. The spin-down density of states is $\rho_{a,\downarrow} = 0.2$. The distance between the two interfaces is $R_{\alpha,\alpha'} = 100$ and the function $G(R)$ is calculated as a function of $R = R_{\alpha,\beta} = R_{\alpha,\alpha'} - R_{\alpha',\beta}$.

7.2.2 Terms of order t^4

Now we consider the terms of order t^4 that couple the two interfaces, namely the terms (34) and (35). Using equations (37–42) we obtain

$$\mathrm{Im}\left[(34) + (35)\right] = \frac{1}{2}\pi^2 t_\alpha^2 t_{\alpha'}^2 \left(\frac{2ma_0^2}{\hbar^2} \right)^3 \left(\frac{a_0}{2\pi} \right)^3 G(R), \quad (46)$$

with

see equations (47–52) above.

The variations of $G(R)$ are shown in Figure 17. It is visible that $G(R)$ is larger in the antiferromagnetic alignment

and therefore in the bulk of the superconductor the superconducting order parameter is larger in the ferromagnetic alignment. This shows that the effect is not a specificity of the local models analyzed in Sections 5 and 6 in which all electrodes are connected to the same site. On the contrary the effect occurs also in the models in Figures 6b and 7b in which the distance between the ferromagnetic electrodes is large compared to the Fermi wave-length.

8 Conclusion

To conclude we have provided a detailed investigation of the proximity effect in multi-connected hybrid structures in which several electrodes are connected to a superconductor. We have pointed out the existence of two mechanisms involved in the determination of the superconducting order parameter. One is related to the existence of an exchange field in the superconductor that was first pointed out in reference [33]. The other mechanism takes place already at a single NS interface. We have first reconsidered FSF heterostructures in which two ferromagnetic electrodes are connected to a superconductor at a distance smaller than the superconducting coherence length. We have found that within a "local" model the superconducting order parameter in the ferromagnetic alignment is larger than the superconducting order parameter in the antiferromagnetic alignment, in agreement with a different model discussed in reference [8]. We have shown that the zero-energy LDOS in the ferromagnetic alignment is larger than the zero-energy LDOS in the antiferromagnetic alignment. In the case where two ferromagnetic and a normal metal electrode are connected to a superconductor we have found that the LDOS in the normal metal depends on the spin orientation in the ferromagnetic electrodes. If the normal metal is replaced by a ferromagnetic metal with a spin-down orientation we have found that $\Delta_{\rm AF} > \Delta_{\rm F}$ for high transparencies and we have provided two analytical models for this behavior (an inversion of the 4×4 Dyson matrix for half-metal ferromagnets and another approach based on a circuit model for partially polarized ferromagnets). We have pointed out that this behavior could be understood from a simple rule stating that for this model the increase of pair correlations in the ferromagnetic electrodes generates a reduction of the superconducting order parameter at the interface. This behavior is confirmed by the exact diagonalizations of the Bogoliubov-de Gennes equations for large values of the exchange field but not for small values of the exchange field.

One explanation to the discrepancy between the two models is that in the Green's function approach only the contribution of energies far above the superconducting gap has been taken into account. This is legitimate if the bandwidth D of the superconductor is much larger than the superconducting gap (in real systems one has typically $D/\Delta \simeq 10^5$). This is justified by the fact that the integral in equation (7) is dominated by the high-energy behavior of the Gorkov function $G^{+,-,1,2}_{\beta,\beta}(\omega) \sim 1/\omega$. On the other hand in the exact diagonalizations of the Bogoliubov-de Gennes Hamiltonian we used small system sizes and replaced the right hand side of equation (7) by a sum over all energy levels. It is thus not surprising that the two procedures (namely the high-energy behavior for large systems and a sum over all energy levels for small systems) can lead to different results in some cases. Another possible source of discrepancy between the two approaches lies in the fact that the ferromagnetic electrodes are one-dimensional and have a finite size in the exact diagonalizations whereas the ferromagnetic electrodes are described by the local density of states of a three dimensional metal in the Green's function approach.

The authors acknowledge fruitful discussions with H. Courtois, D. Feinberg, M. Giroud.

References

1. M.S. Choi, C. Bruder, D. Loss, Phys. Rev. B **62**, 13569 (2000); P. Recher, E.V. Sukhorukov, D. Loss, Phys. Rev. B **63**, 165314 (2001)
2. O. Sauret, D. Feinberg, T. Martin, `cond-mat/0203215`
3. G.B. Lesovik, T. Martin, G. Blatter, Eur. Phys. J. B **24**, 287 (2001)
4. G. Deutscher, D. Feinberg, App. Phys. Lett. **76**, 487 (2000)
5. G. Falci, D. Feinberg, F.W.J. Hekking, Europhys. Lett. **54**, 255 (2001)
6. R. Mélin, J. Phys. Cond. Matt. **13**, 6445 (2001); R. Mélin, *Proceedings of the XXXVIth Rencontres de Moriond*, edited by T. Martin, G. Montambaux, J. Trân Thanh Vân (EDP Sciences, 2001)
7. R. Mélin, D. Feinberg, Eur. Phys. J. B **26**, 101 (2002)
8. V. Apinyan, R. Mélin, Eur. Phys. J. B **25**, 373 (2002)
9. M.J.M. de Jong, C.W. Beenakker, Phys. Rev. Lett. **74**, 1657 (1995)
10. R.J. Soulen *et al.*, Science **282**, 85 (1998)
11. S.K. Upadhyay *et al.*, Phys. Rev. Lett. **81**, 3247 (1998)
12. P. Tedrow, R. Meservey, Phys. Rev. Lett. **26**, 192 (1971); P. Tedrow, R. Meservey, Phys. Rev. B **7**, 318 (1973); R. Meservey, P.M. Tedrow, Phys. Rep. **238**, 173 (1994) and references therein
13. P. Fulde, A. Ferrel, Phys. Rev. **135**, A550 (1964)
14. A. Larkin, Y. Ovchinnikov, Sov. Phys. JETP **20**, 762 (1965)
15. M.A. Clogston, Phys. Rev. Lett. **9**, 266 (1962)
16. E.A. Demler, G.B. Arnold, M.R. Beasley, Phys. Rev. B **55**, 15174 (1997)
17. A.I. Buzdin, L.N. Bulaevskii, S.V. Panyukov, JETP Lett. **35**, 178 (1982) [Zh. Eksp. Teor. Fiz. **35**, 147 (1982)]; A. Buzdin, B. Bujicic, M. Yu. Kupriyanov, Sov. Phys. JETP **74**, 124 (1992) [Zh. Eksp. Teor. Fiz. **101**, 231 (1992)]
18. V.V. Ryazanov, V.A. Oboznov, A. Yu. Rusanov, A.V. Veretennikov, A.A. Golubov, J. Aarts, Phys. Rev. Lett. **86**, 2427 (2001)
19. T. Kontos, M. Aprili, J. Lesueur, X. Grison, Phys. Rev. Lett. **86**, 304 (2001)
20. A.I. Buzdin, M. Yu. Kupriyanov, JETP Lett. **52**, 487 (1990); A.I. Buzdin, M. Yu. Kupriyanov, B. Vujicic, Physica C **185-189**, 2025 (1991)

21. J.S. Jiang, D. Davidović, D.H. Reich, C.L. Chien, Phys. Rev. Lett. **74**, 314 (1995)
22. C.L. Chien, J.S. Jiang, J.Q. Xiao, D. Davidović, D.H. Reich, J. Appl. Phys. **81**, 5358 (1997)
23. L.V. Mercaldo, C. Attanasio, C. Coccorese, L. Maritato, S.L. Prischepa, M. Salvato, Phys. Rev. B **53**, 14040 (1996)
24. J.S. Jiang, D. Davidović, D.H. Reich, C.L. Chien, Phys. Rev. B **54**, 6119 (1996)
25. Th. Muhge, N.N. Garif'yanov, Yu. V. Goryunov, G.G. Khaliullin, L.R. Tagirov, K. Westerholt, I.A. Garifullin, H. Zabel, Phys. Rev. Lett. **77**, 1857 (1996)
    Th. Muhge, K. Westerholt, H. Zabel, N.N. Garif'yanov, Yu. V. Goryunov, I.A. Garifullin, G.G. Khaliullin, Phys. Rev. B **55**, 8945 (1997)
26. M.D. Lawrence, N. Giordano, J. Phys. Cond. Matt. **39**, L563 (1996)
27. V.A. Vas'ko, V.A. Larkin, P.A. Kraus, K.R. Nikolaev, D.E. Grupp, C.A. Nordman, A.M. Goldman, Phys. Rev. Lett. **78**, 1134 (1997)
28. M. Giroud, H. Courtois, K. Hasselbach, D. Mailly, B. Pannetier, Phys. Rev. B **58**, R11872 (1998)
29. V.T. Petrashov, I.A. Sosnon, I. Cox, A. Parsons, C. Troadec, Phys. Rev. Lett. **83**, 3281 (1999)
30. A.T. Filip, B.H. Hoving, F.J. Jedema, B.J. van Wees, B. Dutta, S. Borghs, Phys. Rev. B **62**, 9996 (2000)
31. M. Giroud, K. Hasselbach, H. Courtois, D. Mailly, B. Pannetier, `cond-mat/0204140`
32. I. Baladie, A. Buzdin, N. Ryzhanova, A. Vedyayev, Phys. Rev. B **63**, 054518 (2001); I. Baladie, A. Buzdin, `cond-mat/0209466`
33. P.G. de Gennes, Phys. Lett. **23**, 10 (1966)
34. G. Deutscher, F. Meunier, Phys. Rev. Lett. **22**, 395 (1969)
35. J.J. Hauser, Phys. Rev. Lett. **23**, 374 (1969)
36. E. Vecino, A. Martin-Rodero, A. Levy Yeyati, Phys. Rev. B **64**, 184502 (2001)
37. P.G. de Gennes, *Superconductivity of Metals and Alloys* (Benjamin, New York, 1966)
38. N. Stefanakis, Phys. Rev. B **66**, 024514 (2002)
39. P.G. de Gennes, D. Saint-James, Phys. Lett. **4**, 151 (1963)
40. J.C. Cuevas, A. Martin-Rodero, A. Levy Yeyati, Phys. Rev. B **54**, 736 (1996)
41. K. Halterman, O.T. Valls, Phys. Rev. B **65**, 014509 (2002)
42. M. Tinkham, *Introduction to superconductivity* (McGraw-Hill, 1996)
43. G. Deutscher, F. Meunier, Phys. Rev. Lett. **22**, 395 (1969)
44. J.J. Hauser, Phys. Rev. Lett. **23**, 374 (1969)
45. Y.A. Genenko, Y.A. Ivanchenko, Theor. Math. Phys. **69**, 1056 (1986)
46. N. Moussy, H. Courtois, B. Pannetier, Europhys. Lett. **55**, 861 (2001)